Lehrstuhl für Bildverarbeitung
Institute of Imaging & Computer Vision

High Dynamic Range Images as a Basis for Detection of Argyrophilic Nucleolar Organizer Regions Under Varying Stain Intensities

André A. Bell and Jens N. Kaftan and Til Aach and Dietrich Meyer-Ebrecht and Alfred Böcking

Institute of Imaging and Computer Vision
RWTH Aachen University, 52056 Aachen, Germany
tel: +49 241 80 27860, fax: +49 241 80 22200
web: www.lfb.rwth-aachen.de

in: IEEE International Conference on Image Processing, ICIP 2006. See also BIBTEX entry below.

BIBTEX:

```
@inproceedings{BEL06b,
  author    = {Andr\'{e} A. Bell and Jens N. Kaftan and Til Aach and
               Dietrich Meyer-Ebrecht and Alfred B\"{o}cking},
  title     = {{H}igh {D}ynamic {R}ange {I}mages as a {B}asis
               for {D}etection of {A}rgyrophilic {N}ucleolar {O}rganizer {R}egions
               {U}nder {V}arying {S}tain {I}ntensities},
  booktitle = {IEEE International Conference on Image Processing, ICIP 2006},
  publisher = {IEEE},
  year      = 2006,
  pages     = {2541--2544},
}
```


document created on: October 18, 2006
created from file: hdragnor.tex
cover page automatically created with CoverPage.sty
(available at your favourite CTAN mirror)

RWTH AACHEN
RHEINISCH-WESTFÄLISCHE TECHNISCHE HOCHSCHULE AACHEN

HIGH DYNAMIC RANGE IMAGES AS A BASIS FOR DETECTION OF ARGYROPHILIC NUCLEOLAR ORGANIZER REGIONS UNDER VARYING STAIN INTENSITIES

A. A. Bell[1], *J. N. Kaftan*[1], *T. Aach*[1], *D. Meyer-Ebrecht*[1], *A. Böcking*[2]

Email: {ab,jk,ta,me}@lfb.rwth-aachen.de
[1]Institute of Imaging and Computer Vision, RWTH Aachen University, Germany
[2]Institute for Cytopathology, Heinrich-Heine-University, Düsseldorf, Germany

ABSTRACT

Silver staining of cytopathologic specimens offers advantages in cancer diagnostics. A difficulty with such stained cell specimens is the very high dynamic range needed by the imaging system to appropriately cover the varying stain intensities. Beside those images of cell nuclei that can be used for the diagnostic interpretation, there are nuclei that appear too dark to observe their relevant properties, the so-called argyrophilic nucleolar organizer regions (AgNORs), which appear as spot-like areas darker than their immediate surroundings. We therefore show how high dynamic range images of nuclei can help to correctly segment the AgNORs. To this end, we acquire a sequence of differently exposed images, which are then combined into a high dynamic range image. Based on the dynamic range of the image signal within the segmented cell area, we compute another image which provides optimal contrast over this area of interest. To further increase the contrast for dark objects, a suitable nonlinear point transform is simultaneously applied. We provide examples of the thus generated images and their corresponding segmentations.

1. INTRODUCTION

The earlier cancer is detected, the larger is the chance for successful treatment. Moreover, the curative costs are mostly lower, if a tumor is diagnosed earlier. Both requires an early cancer diagnosis. We therefore seek to diagnose cancer before macroscopically visible symptoms appear. In addition, the methods used in such an early screening must not subject patients to stress and thus have to be noninvasive.

Since cancer starts from single cells, cytopathological and molecular cell analyses are the methods of choice. Cytopathologic specimens can be taken, e.g., with tiny brushes from mucosae or by Fine Needle Aspiration Biopsies (FNABs), from different organs. This provides specimens without hurting surrounding tissue. Based on the cells in these specimens it is possible to detect cancer earlier, painless and without stress for the patient [1].

The project is supported by the Viktor and Mirka Pollak Fund for Biomedical Engineering.

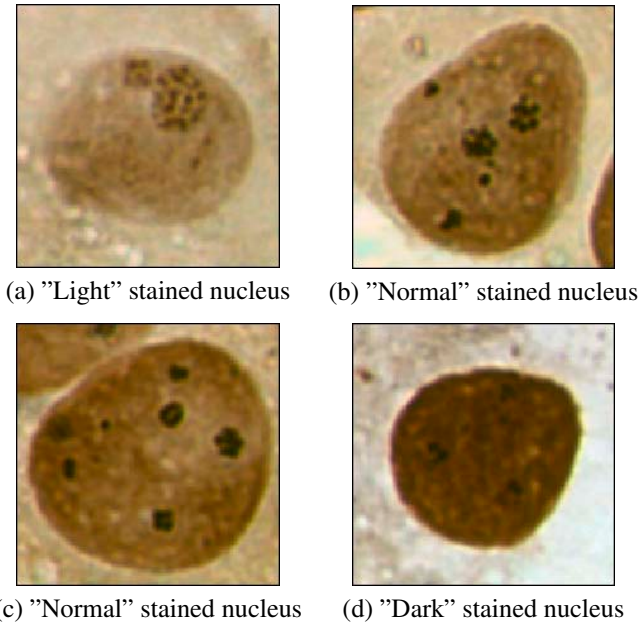

(a) ”Light” stained nucleus (b) ”Normal” stained nucleus

(c) ”Normal” stained nucleus (d) ”Dark” stained nucleus

Fig. 1. Images of differently intensive stained cell nuclei of pleura effusion from the same specimen, i.e., from one slide. Within the cell nuclei of the images (a), (b), and (c) the AgNORs, which appear as dark spots, can be observed quite easily. In the nucleus of image (d) the contrast is very low and therefore the AgNORs are nearly undetectable.

For cancer diagnostics based on cells many methods have been developed, e.g., confocal laserscanning microscopy, fluorescence microscopy, and DNA flowcytometry [2, 3]. In our case we employ visible-light brightfield microscopy, i.e., the cells must be stained. Different stains reveal different information of the cells under scrutiny. Stains like Papanicolaou or May-Grünwald-Giemsa reveal the cell morphology, whereas Feulgen stains the DNA of the cell stoichiometrically, which is used for DNA Image Cytometry. We focus in this paper on the silver stain.

Silver staining of cells has been shown to be useful for cancer diagnostics [4, 5]. Silvernitrate stains the nucleolar

organizer regions (AgNORs) of the cells, which then appear as dark spots within the cell nucleus (see figure 1). Each cell contains at least one AgNOR, which are conventionally counted. Recently it could be shown that measuring the area of the AgNORs further improves the diagnostic accuracy [6], for instance to preoperatively distinguish malignant carcinoma of the thyroid gland from benign adenoma.

A challenge for automatic AgNOR segmentation is the low homogeneity of the staining results, which leads to strong variations in the staining intensities of different cells. This effect can even be observed within one slide (see figure 1).

From an imaging and image processing point of view, the staining process leads to cell specimens requiring a larger dynamic range than existing digital cameras are able to provide. Simply increasing the amount of light delivered from the microscope lamp or increasing the exposure time of the camera might make the very dark stained cells accessible to the diagnostic interpretation. The lighter stained cells, however, are then lost for the diagnosis because of saturation of the camera. We therefore propose to use high dynamic range images, which require the acquisition of differently exposed images from the cells to be analyzed.

The images were acquired with a JAI CV-M90 3CCD camera mounted on top of a Leica DMLA microscope. A 63x objective lens with numerical aperture $\mathsf{NA} = 1.32$ has been used for the acquisition of the images. The resulting pixelsize is $\Delta x \approx 0.1 \mu m$.

Our database contains 42 specimens of pleura effusions, 63 specimens of Fine Needle Aspiration Biopsies of the thyroid gland and 40 specimens of the oral mucosa. For each specimen, images of cells under suspicion have been acquired in Papanicolaou or May-Grünwald-Giemsa stain for morphological review. These specimens were destained and stained again according to Feulgen to obtain DNA-measurements of the same cells after relocation [7]. Finally these specimens were once more destained and stained with silvernitrate. This sums up to $69,038$ images or about $116,466$ cells verified by our medical partner. Of these images $16,918$ were captured in silver stain. The AgNORs within $12,911$ cells were manually counted by our medical partner. This will be complemented in our current work by manual segmentation of AgNORs as a goldstandard for validation.

2. HIGH-DYNAMIC-RANGE IMAGING AND SEGMENTATION

In a series of differently exposed images of the same scene, each image reveals different details (see figure 2). These images are mappings from the quantity of light q, incident on the imaging sensor, onto the gray- or colorvalues in the image, by a mostly nonlinear camera transfer function (CTF) denoted by f. To combine these images into one high dynamic range (HDR) image, one first has to apply the inverse f^{-1} of f to each image to undo the nonlinearities of f.

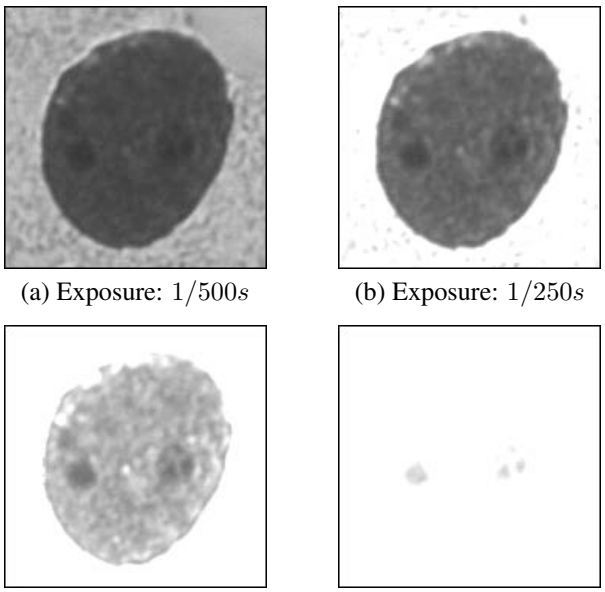

(a) Exposure: $1/500s$ (b) Exposure: $1/250s$

(c) Exposure: $1/100s$ (d) Exposure: $1/50s$

Fig. 2. Four images of the same nucleus differing only in exposure. Only the red-channel of the color-images is shown, since the AgNORs can be observed best in that channel.

Different methods [8, 9, 10, 11] have been published to estimate f and tonally align such images into a high dynamic range image. The function

$$f(q) = \alpha + \beta q^{\gamma} \tag{1}$$

is a good model for the CTF of a JAI CV-M90 3CCD camera [12]. From [8] it follows that for each image f_i, acquired with a different exposure setting k_i, an estimate for the quantity of light $\hat{q}_i$ incident on the imaging sensor is given by

$$\hat{q}_i = \frac{1}{k_i} \hat{f}^{-1}(f_i) \tag{2}$$

where α and γ, and thus $\hat{f}^{-1}$, were estimated from the differently exposed images f_i as described in [8]. The parameter β is a scaling factor which can be chosen arbitrarily. It has been shown that, using this method, the parameters α and γ can be estimated accurately for this camera [12]. The exposure series is now combined into one estimate for the quantity of light falling on the imaging sensor by

$$\hat{q} = \frac{\sum_i \hat{c}_i \hat{q}_i}{\sum_i \hat{c}_i} \tag{3}$$

where $\hat{c}_i$ is a certainty function used for weighting the estimates $\hat{q}_i$ with respect to the accuracy of the ranges represented within the different images f_i. Since the quantization noise is low and consequently the accuracy high for those ranges where the slope of the CTF is high, we have chosen this function to be the derivative of the CTF [8].

What is the difference between this high dynamic range image and the set of images with different exposure settings? Depending on the camera and microscope setup, the images f_i are arbitrary large "windows" of the dynamic range of the scene, while quantities of light greater than this window are represented as saturated pixels. As an example, see figure 2. Since the dynamic range of the AgNORs varies heavily depending on the staining process, the optimal camera setting, which reproduces the contrast of the region of interest best, is unknown. In addition blooming effects might compromise the region of interest. The blooming effect of the CCD sensor partially erodes the border areas of those regions which are close to saturated pixels. This effect is partially removed in the combined HDR image, since the certainty function drops to zero for saturated pixels.

The best image for the detection of the AgNORs is that one where the dynamic range from the lowest to the highest quantity of light within the cell nucleus is represented by the full range of values of our image (here: 8bit). Towards this end, we exploit the fact that within our system, a segmentation of the cell nucleus is available from the analysis of another stain (usually Feulgen), which is readily coregistered to the image [7]. Let us denote the minimum and maximum quantity of light within the nucleus by q_{min} and q_{max} respectively. We now seek to find parameters α, β and γ for the camera transfer function (1) of a *virtual camera* f_{virt} that maps the range $R_{in} = [q_{min}; q_{max}]$ of the HDR-image to the range $R_{out} = [0; 255] = [g_{min}; g_{max}]$ of a windowed image.

For a given γ this means

$$f_{virt}(q_{max}) = g_{max} = \alpha + \beta {q_{max}}^{\gamma} \quad (4)$$

$$f_{virt}(q_{min}) = g_{min} = \alpha + \beta {q_{min}}^{\gamma} \quad (5)$$

yielding

$$\beta = \frac{g_{max} - g_{min}}{{q_{max}}^{\gamma} - {q_{min}}^{\gamma}} \quad \wedge \quad \alpha = g_{min} - \beta {q_{min}}^{\gamma} \quad (6)$$

Choosing $\gamma = 1$ will give a linear mapping of the range R_{in} onto the range R_{out}. Since we are interested in dark spots, we can increase their contrast even further by setting $\gamma \in (0, 1.0)$, e.g., $\gamma = 0.5$. This consequently expands the lower values and compresses the higher values.

We now have obtained images that make use of the full dynamic range of 8 bit for the imaging of the cell nucleus. Simultaneously the darker parts of the image are represented by more quantization steps. As an example, figure 3 (a) shows the red-channel of three high dynamic range images after this mapping.

These windowed images can now be segmented. Our segmentation uses the mean shift algorithm [13] which provides consistently good results in a variety of applications, including clustering, segmentation and filtering [14, 15].

The mean shift technique, a nonparametric density estimation, is based on a kernel density estimator, known as the

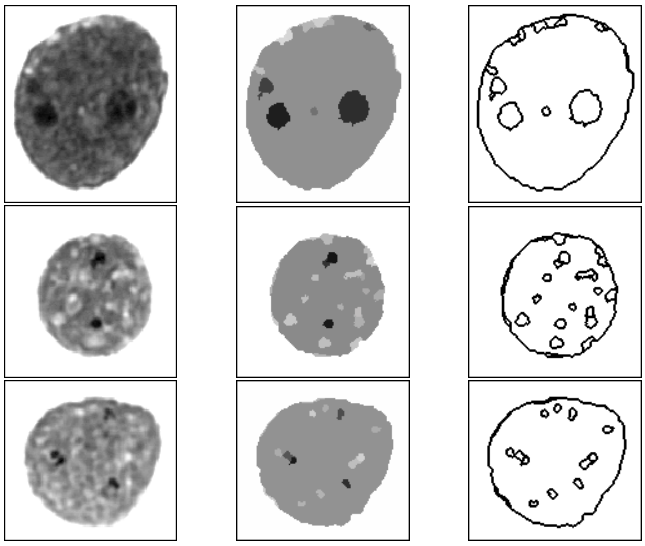

(a) (b) (c)

Fig. 3. Column (a) shows the red channel of the windowed images. In column (b) the mean-shift segmented images are shown. The color of each segment is defined by the color of the corresponing mode of this region. Column (c) shows the segment boundaries. The first cell is taken from the thyroid gland while the others are taken from pleura effusions. The falsely detected non-AgNOR segments can be easily removed by comparing their mean values to the mean of the nucleus background.

Parzen Density Estimate [13]:

$$\hat{f}(\mathbf{x}) = \frac{1}{Nh^d} \sum_{i=1}^{N} K\Big(\frac{\mathbf{x} - \mathbf{x}_i}{h}\Big) \quad (7)$$

Here, N equals the number of d-dimensional vectors $\mathbf{x}_1..\mathbf{x}_n$. The parameter h is the window radius of the used kernel K.

It can be shown that the gradient of the Parzen Density Estimate using, e.g., an Epanechnikov kernel,

$$K_E(\mathbf{x}) = \begin{cases} \frac{1}{2} c_d^{-1} (d+2)(1 - \|\mathbf{x}\|^2) & \|\mathbf{x}\| \leq 1 \\ 0 & otherwise \end{cases} \quad (8)$$

becomes

$$\hat{\nabla} f(\mathbf{x}) = \frac{N_x (d+2)}{N c_d h^{d+2}} \mathbf{m}_h(\mathbf{x}), \;\; \mathbf{m}_h(\mathbf{x}) = \frac{1}{N_x} \sum_{\mathbf{x}_i \in S_h(\mathbf{x})} (\mathbf{x}_i - \mathbf{x})$$

where N_x is the number of data vectors $\mathbf{x}_i$ within the window S_h. The constant c_d ensures that the kernel K_E integrates to 1, and $\mathbf{m}_h(\mathbf{x})$ is the mean shift vector which is proportional to the normalized gradient density estimate [13, 15]. The mean shift vector thus always points towards the direction of maximum increase in the density. By iteratively calculating the

mean shift vector for one position with given radius h and afterwards shifting the kernel window by this vector, this procedure will converge to a point with zero gradient [15], i.e., to a mode corresponding to the initial position. The mean shift procedure is hence an effective algorithm for mode seeking in a density distribution without prior calculation of this distribution.

For a segmentation application the data vectors $\mathbf{x}_i$ are composed of the spatial and the color information of each pixel. In this case it is reasonable to choose an anisotropic kernel window, which differs in size in spatial domain and range domain, i.e., color space. Using a radius h_s in spatial and h_r in the range domain, the anisotropic kernel becomes:

$$K_{h_s,h_r}(\mathbf{x}) = \frac{C}{h_s^2 h_r^p}\, k\left(\left\|\frac{\mathbf{x}_s}{h_s}\right\|^2\right) k\left(\left\|\frac{\mathbf{x}_r}{h_r}\right\|^2\right) \qquad (9)$$

where $\mathbf{x}_s$ is the spatial and $\mathbf{x}_r$ the range part of a data vector of dimension $d = p + 2$, and $k(\cdot)$ the common kernel-profile [14, 15]. Since color-images normally exhibit three color-channels it follows that $p = 3$ and $p = 1$ for grayscale-images, respectively. For segmentation, the mean shift procedure is first performed for each pixel of the input image. Afterwards the corresponding modes, which are closer than h_s and h_r to each other are grouped together to one segment. Regions smaller than a certain size might be eliminated [15].

3. RESULTS AND DISCUSSION

AgNORs are dark spots within the cell nuclei and their segmentation is a useful tool for early cancer diagnosis. Based on the observation that single-exposure images do not provide sufficient dynamic range, we acquire exposure series from which high dynamic range images are computed. In our setup the nucleus segmentation is known from prior steps, which enables the definition of a *virtual camera* which maps the region of interest into one image using the complete available dynamic range. The mapping is based on an analysis of the intensity range within the areas relevant for diagnosis, i.e., the cell nucleus.

The thus obtained images can be used as a basis for automatic detection of the nucleolar organizer regions of the cells. Performing the segmentation on these images is superior to segmentation on common low dynamic range images since all accessible information through each exposure series is combined into one image. AgNOR segmentation results by mean shift on these images are shown in figure 3 and have so far been found satisfactory by our medical partner.

The falsely detected non-AgNOR segments can be easily removed by comparing their mean values to the mean of the cell background. A validation of the segmentation performance against a goldstandard will follow as soon as manual segmentations are available.

4. REFERENCES

[1] A. Böcking, J. Stockhausen, and D. Meyer-Ebrecht, "Towards a single cell cancer diagnosis. Multimodal and Monocellular Measurements of Markers and Morphology (5M)," *Cellular Oncology*, vol. 26, pp. 73–79, 2004.

[2] S. Taylor, J. Blatt, J. Costantino, M. Roederer, and R. F. Murphy, "Flow Cytometric DNA Analysis of Neuroblastoma and Ganglioneuroma: a 10-year Retrospective Study.," *Cancer*, vol. 62, pp. 749–754, 1988.

[3] H. Motherby, N. Pomjanski, M. Kube, A. Boros, T. Heiden, B. Tribukait, and A. Böcking, "Diagnostic DNA-flow- vs. -image-cytometry in effusion cytology," *Anal Cell Pathol*, vol. 24 (1), pp. 5–15, 2002.

[4] J. Rüschoff, C. H. Prasser, T. Cortez, H. M. Höhne, W. Hohenberger, and F. Hofstädter, "Diagnostic value of AgNOR staining in follicular cell neoplasms of the thyroid: Comparison of evaluation methods and nucleolar features," *AM J Surg Pathol*, vol. 17, pp. 1281–1288, 1993.

[5] T. W. Remmerbach, H. Weidenbach, C. Muller, A. Hemprich, N. Pomjanski, B. Buckstegge, and A. Böcking, "Diagnostic value of nucleolar organizer regions (AgNORs) in brush biopsies of suspicious lesions of the oral cavity," *Anal Cell Pathol*, vol. 25 (3), pp. 139–146, 2003.

[6] D. Slowinska-Klencka, M. Klencki, B. Popowicz, and A. Lewinski, "AgNOR quantification in the diagnosis of follicular pattern thyroid lesions," *Anal Quant Cytol Histol*, vol. 25 (6), pp. 347–352, 2004.

[7] T. Würflinger, J. Stockhausen, D. Meyer-Ebrecht, and A. Böcking, "Robust Automatic Coregistration, Segmentation, and Classification of Cell Nuclei in Multimodal Cytopathological Microscopic Images," *Computerized Medical Imaging and Graphics*, vol. 28, pp. 87–98, 2004.

[8] S. Mann, "Comparametric equations with practical applications in quantigraphic image processing," *IEEE Trans. on Image Processing*, vol. 9 (8), pp. 1389–1406, 2000.

[9] P. E. Debevec and J. Malik, "Recovering High Dynamic Range Radiance Maps from Photographs," in *Proceedings ACM SIGGRAPH*, 1997, pp. 369–378.

[10] T. Mitsunaga and S. K. Nayar, "Radiometric self calibration," in *IEEE Conference on Computer Vision and Pattern Recognition. CVPR*, 1999, vol. 1, pp. 374–380.

[11] F. M. Candocia, "Analysis and enhancements to piecewise linear comparametric image registration," *IEEE Trans. on Image Processing*, vol. 14 (2), pp. 181–188, 2005.

[12] A. A. Bell, J. N. Kaftan, D. Meyer-Ebrecht, and T. Aach, "An Evaluation Framework for the Accuracy of Camera Transfer Functions Estimated from Differently Exposed Images," in *7th Southwest Symposium on Image Analysis and Interpretation, SSIAI*, 2006, pp. 168–172.

[13] K. Fukunaga and L. D. Hostetler, "The Estimation of the Gradient of a Density Function, with Applications in Pattern Recognition," *IEEE Trans. on Information Theory*, vol. 21 (1), pp. 32–40, 1975.

[14] Y. Cheng, "Mean Shift, Mode Seeking, and Clustering," *IEEE Trans. on Pattern Analysis and Machine Intelligence*, vol. 17 (8), pp. 790–799, 1995.

[15] D. Comaniciu and P. Meer, "Mean Shift: A Robust Approach Toward Feature Space Analysis," *IEEE Trans. on Pattern Analysis and Machine Intelligence*, vol. 24 (5), pp. 603–619, 2002.